FLUCOME 2009
10th International Conference on Fluid Control, Measurements, and Visualization
August 17–21, 2009, Moscow, Russia

# NUMERICAL SIMULATION OF ZERO-NET-MASS JET FLOW

Qian Weiqi[1] He Kaifeng[2] Liu Gang[3] Chen Zuobin[4]

## ABSTRACT

Zero-Net-Mass Jet(ZNMJ) flow is an important aspect of active flow control research. By solving unsteady RANS with Finite Volume Method and dual-time technique, the numerical method to simulate the ZNMJ flow field is developed and applied to analyze the flow characteristics in three typical configurations of ZNMJ device. For the first configuration, the influence of Boundary Condition(BC) setting, the effect of Geometric Conservation Law(GCL) in the dynamic grid deformation technique are studied. And it is found that the moving boundary of ZNMJ can be simplified to specify a time-varying velocity value on the fixed grid and if the dynamic grid deformation technique is used the utilization the GCL is necessary in simulation. For the second 2D and third 3D configuration, the flow fields are computed and compared to respective PIV experimental results. It is shown that the calculated results agree with the experimental results substantially and some difference exists for the "suction" phase of the ZNMJ, which needs further investigation. However, generally speaking, this developed numerical method is a feasible tool to depict the flow field of ZNMJ.

**Keywords: Zero-Net-Mass Jet flow, numerical simulation, flow control, unsteady, dynamic grid technique**

## INTRODUCTION

Flow control is one of leading area of research in aviation and fluid dynamics, and with the emergence and development of microfabricated electromechanical systems(MEMS), a typical MEMS design, Zero-Net-Mass Jet(ZNMJ) or synthetic jet, is showing its promising ability to provide solutions that avert the use of more traditional complex mechanical, electrical and pneumatic control systems for aerodynamic enhancement and active control. In general, ZNMJ results from oscillating a diaphragm in an enclosed rigid cavity having an orifice. The diaphragm of ZNMJ actuator is activated electrostatically, electromagnetically, or through the use of piezo-electric material and the synthesized external jet-like flow results from the entrainment of the surrounding ambient fluid as a result of the fluctuations in the pressure along the axis of the jet. The unique characteristics of the ZNMJ flow-field and the working attributes of the actuators make ZNMJ actuators suitable for a large class of applications, including jet vectoring, control of separation, enhanced mixing, reduction of wall friction, virtual shaping, micro-pump, and so on. Flow control approaches that use ZNMJs have become a remarkable and important active flow

[1] Corresponding author: China Aerodynamic Research and Development Center, Mianyang Sichuan 621000, China
[2] China Aerodynamic Research and Development Center, Mianyang Sichuan 621000, China
[3] China Aerodynamic Research and Development Center, Mianyang Sichuan 621000, China
[4] China Aerodynamic Research and Development Center, Mianyang Sichuan 621000, China

control technology for recent decade (Hassan, 2001). However, the flow of ZNMJ exhibits complex unsteady phenomena of vortex generating, shedding and merging. In order to investigate the flow physics of ZNMJ, many experimental works such as Tang & Zhong(2006) have been conducted and it's necessary to develop a numerical tool to study the ZNMJ flow and compare with these experimental results.

## NUMERICAL METHOD

The control equation of the ZNMJ flow field is the unsteady Reynolds-Averaged Navier-Stokes equations, and its nondimensional form can be written in curvilinear coordinate system (Zhu, 1998),

$$\frac{\partial \hat{Q}}{\partial t}+\frac{\partial \hat{E}}{\partial \xi}+\frac{\partial \hat{F}}{\partial \eta}+\frac{\partial \hat{G}}{\partial \varsigma}=\frac{1}{\mathrm{Re}}\left(\frac{\partial \hat{E}_v}{\partial \xi}+\frac{\partial \hat{F}_v}{\partial \eta}+\frac{\partial \hat{G}_v}{\partial \varsigma}\right) \tag{1}$$

with $\hat{Q}=J^{-1}\begin{pmatrix}\rho\\ \rho u\\ \rho v\\ \rho w\\ e\end{pmatrix}$ ; $\hat{E},\hat{F},\hat{G}=J^{-1}\begin{pmatrix}\rho V_n\\ \rho u V_n+l_x p\\ \rho v V_n+l_y p\\ \rho w V_n+l_z p\\ (e+p)V_n-l_t p\end{pmatrix}$ ; $V_n=ul_x+vl_y+wl_z$ ; $l_t=-l_x\dot{x}-l_y\dot{y}-l_z\dot{z}$ ; and $l$ corresponds to $\xi$, $\eta$, $\zeta$ for the three momentum equations respectively. $\hat{E}_v$, $\hat{F}_v$, $\hat{G}_v$ are viscous terms and the turbulence effect is taken account by $k$-$\omega$ SST two-equation turbulence model (Menter, 1993).

$$\frac{D\rho k}{Dt}=\frac{\partial}{\partial x_j}\left[\left(\mu+\sigma_k\mu_t\right)\frac{\partial k}{\partial x_j}\right]+\tau_{ij}\frac{\partial u_i}{\partial x_j}-\beta^*\rho\omega k$$

$$\frac{D\rho\omega}{Dt}=\frac{\partial}{\partial x_j}\left[\left(\mu+\sigma_\omega\mu_t\right)\frac{\partial \omega}{\partial x_j}\right]+\frac{\gamma}{\nu_t}\tau_{ij}\frac{\partial u_i}{\partial x_j}-\beta\rho\omega^2+2\left(1-F_1\right)\rho\sigma_{\omega 2}\frac{1}{\omega}\frac{\partial k}{\partial x_j}\frac{\partial \omega}{\partial x_j}$$

$$\nu_t=\frac{a_1 k}{\max\left(a_1\omega\,;\,\Omega F_2\right)};\quad a_1=0.31;\quad \tau_{ij}=-\rho\overline{u_i'u_j'} \tag{2}$$

Where $\beta$, $\gamma$, $\sigma_k$, $\sigma_\omega$ are model parameters; $F_1$ and $F_2$ are blending functions.

The equations(1)(2) can be discretized simutaneously with Finite Volume Method, and the implicit dual-time technique similar to Dubuc(1998) is applied for the unsteady term. i.e., the temporal derivative in the pseudo-time iteration is treated by LU-SGS technique and the temporal derivative in the physical time step is discretized with the following Three-Layer-Fully Implicit scheme of second order accuracy,

$$\frac{\partial \hat{Q}}{\partial t}=\frac{3\hat{Q}^{n+1}-4\hat{Q}^{n}+\hat{Q}^{n-1}}{2\Delta t} \tag{3}$$

where the superscripts of "$n$-1", "$n$", "$n$+1" are the physical time step index and $\Delta t$ is the physical time step size. For spatial derivative terms in the unsteady RANS, the convective and dissipative terms are discretized with Roe's FDS scheme and central difference respectively.

In addition, in order to simulate the oscillation of the diaphragm in the ZNMJ device, the dynamic

grid technique may be used. After the term of $\partial \hat{Q}/\partial t$ in eq.(1) is written as

$$\partial \hat{Q}/\partial t = J^{-1}(\partial Q/\partial t) + Q(\partial J^{-1}/\partial t) \tag{4}$$

It can be seen that when the grid is moving, there comes out a term of $\partial J^{-1}/\partial t$ indicating the unsteady changing of grid volume and this term should be calculated with the following Geometric Conservation Law(GCL),

$$(\partial J^{-1}/\partial t) = -[(\xi_t/J)_\xi + (\eta_t/J)_\eta + (\zeta_t/J)_\zeta] \tag{5}$$

## NUMERICAL EXAMPLES AND DISCUSSION

### Numerical Example 1

Firstly, a ZNMJ device configuration shown in Fig.1 is numerically simulated with aforementioned method. In this configuration, the width of jet exit is 1mm and AB is vibrating with $\Delta y = 0.002(100 - x^2)\sin(2\pi ft)$ and $f$=150Hz. For this configuration, the computational domain is meshed with three parts of 121×81, 25×17 and 89×17 and three calculations are performed to study the influence of Boundary Condition(BC) setting, the effect of Geometric Conservation Law(GCL) in the dynamic grid deformation technique. In the first calculation, the dynamic grid technique is not used and the vibration of AB is simplified to be a time-varying periodic velocity BC on the fixed grid as $v = \Delta\dot{y} = 0.002(100 - x^2)2\pi f \cos(2\pi ft)$. In the second calculation, the dynamic grid technique is used but the GCL is not employed and the vibration of AB is treated as a BC of moving wall. In the third calculation, the GCL is employed in the dynamic grid technique. The calculated histories of the velocity at the center of jet exit of these three calculations (denoted as "Periodic BC", "Dynamic grid", "Dynamic grid with GCL" respectively) are compared in Fig.2. From this figure, the following three conclusions can be drawn. First, all the results show a periodic oscillation of the jet velocity. Second, there is a great difference between the results of oscillation amplitude in the second and third simulation, that means the utilization the GCL in the dynamic grid deformation technique is necessary. Third, the calculated result of dynamic grid deformation technique together with GCL is nearly identical to the result calculated by specifying a BC of time-varying velocity value to the moving boundary on the fixed grid, so that this velocity BC specification method can be applied to complex configuration calculation for simplicity.

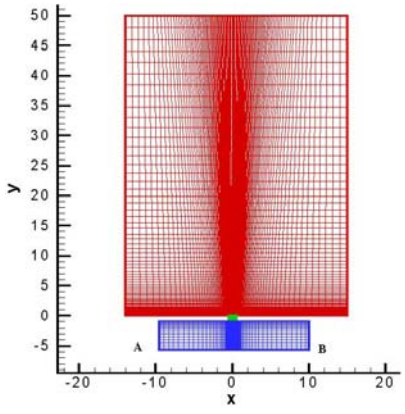


**Fig. 1. 2D ZNMJ device configuration**

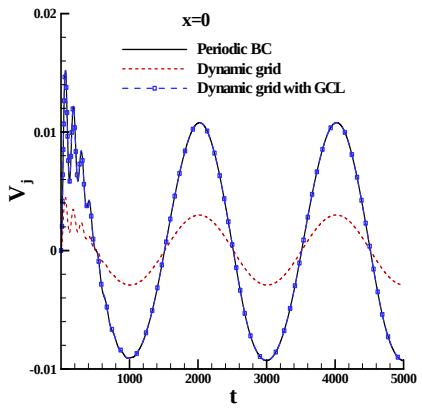


**Fig. 2 Comparison of velocity history**

In Fig.3, the vorticity contour of the flow field at two moments in a period of AB oscillation are presented. The left figure corresponds to the maximum place of AB oscillation and a pair of vortex is generated at the exit and shed downstream. While in the right figure corresponding to the minimum place of AB oscillation, a pair of vortex is generate and moves in the cavity. The whole flow field exhibits a complex flow character of unsteady vortex movement.

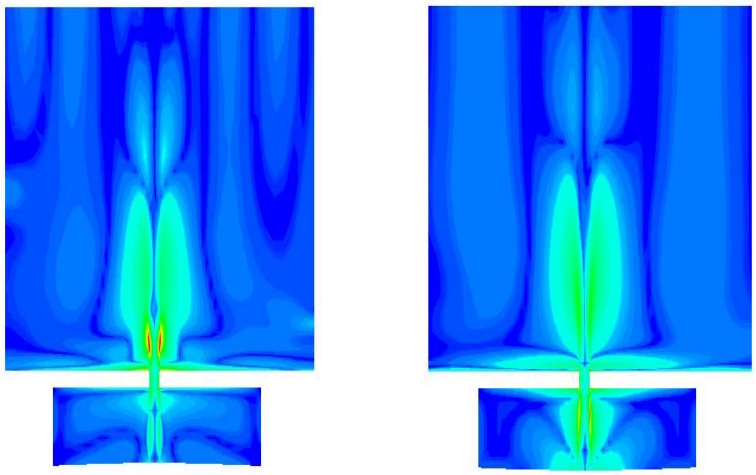

**Fig. 3. Vorticity contour of the ZNMJ flow field at two moments**

**Numerical Example 2**

Secondly, another two-dimensional ZNMJ device configuration made by Luo (2006) is shown in Fig.4 and numerically simulated. The ZNMJ is generated by the vibration of AB and thanks to the third conclusion of the example 1 the flow field is simulated by specifying a velocity BC for AB as $u(y) = 0.35[1.0 - (y+27)^2/23^2]2\pi f \cos(2\pi ft)$ where $f$=500Hz. When the calculated results are got, they are compared with the Particle-Image-Velocimetry experimental results. First, the y-direction velocity at the point (0,1) in a period is compared with the experimental result in Fig.5. It can be seen from this figure that the calculated result agrees with the experimental result quantitatively. Especially, if the jet is divided into two phases of blow and suction, it can be seen that the calculated velocity peak of the blow phase matches better to the experimental result than the suction phase. Second, the y-direction velocities along the line of $x$=0 at two nondimensional time of t*=0.25 and t*=0.75 are compared with experimental result in Fig.6. It can be seen that at t*=0.25, the calculated result agree well with the experimental result in the range of $y$<10 and calculated result is a bit larger than the experimental result in the range of $y$>10. As for t*=0.75, the calculated result agree well with the experimental result in the range of $y$>5 but in the range of $y$<5, there are some difference between the calculated and experimental results, which is consistent with the suction phase result in Fig.5. Third, the y-direction velocity and x-direction velocity along the line of $y$=1 at two time of t*=0.25 and t*=0.75 are further compared with experimental result in Fig.7 and Fig.8. it can be seen from Fig.7 that at t*=0.25 the calculated result agree well with the experimental result while at t*=0.75, there exist a significant difference between the calculated and experimental results. As for the x-direction velocity comparison, the calculated result also agrees with the experimental result substantially.

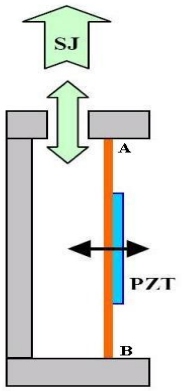


**Fig. 4. Sketch of 2D ZNMJ device**

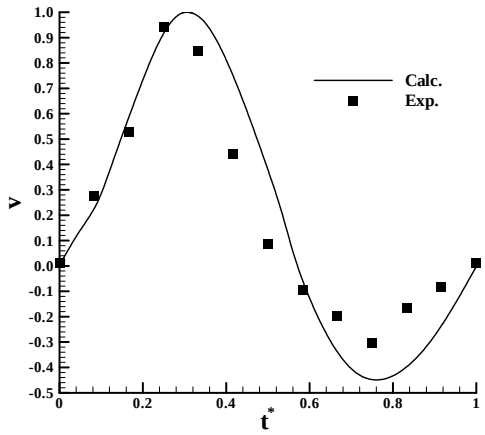


**Fig.5 Comparison of y-direction velocity at point (0,1)**

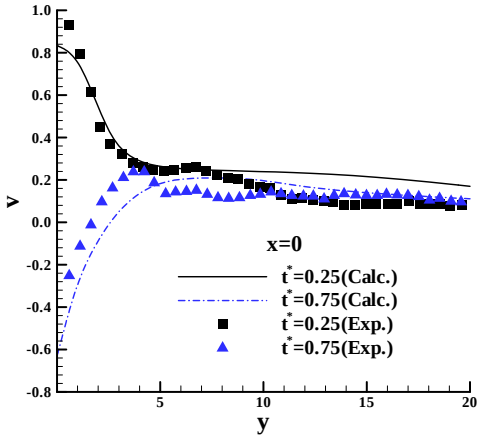


**Fig.6 Comparison of y-direction velocity along the line of x=0 at two time**

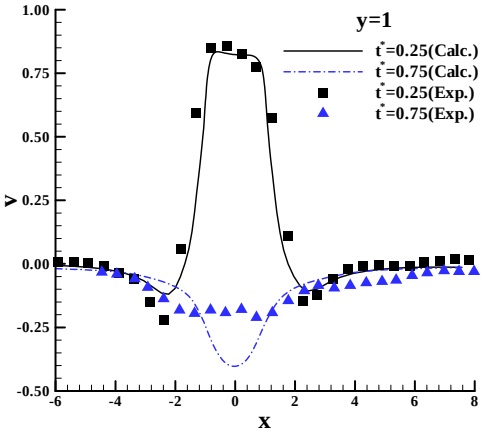


**Fig.7 Comparison of y-direction velocity along the line of y=1**

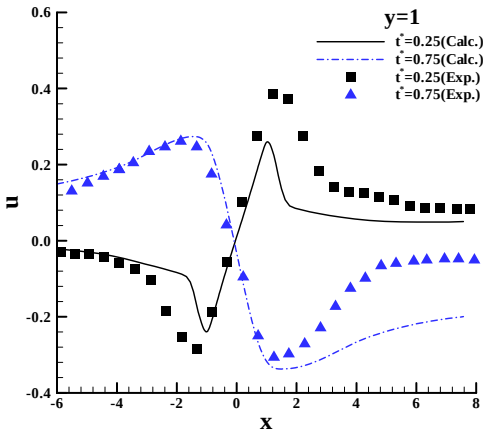


**Fig.8 Comparison of x-direction velocity along the line of y=1**

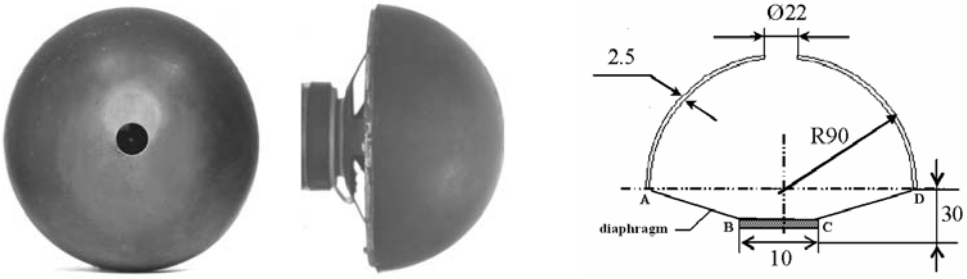


**Fig. 9 Three dimensional ZNMJ device**

**Numerical Example 3**

The third example is a three dimensional ZNMJ device made by Gu&Ming(2005) in the Nanjing University of Aeronautics and Astronautics shown in Fig.9. In this device, a 6.5 inch loudspeaker with a power of 10W is located in a hemisphere of diameter 175mm, and the moving part of ABCD in the loudspeaker responds to the input signal and vibrates to generate a ZNMJ at the top exit of the

hemisphere. The main moving part of ABCD is the sinusoidal movement of BC and AB and CD just moves following BC, i.e.,

$$\Delta z = \begin{cases} d_{\max}\sin(2\pi ft+\phi) & ;\ point\ in\ \mathrm{BC} \\ \dfrac{r_A - r}{r_A - r_B} d_{\max}\sin(2\pi ft+\phi) & ;\ point\ in\ \mathrm{AB}\ and\ \mathrm{CD} \end{cases} \tag{6}$$

where $f$=100Hz and $d_{max}$=0.45mm. To treat this configuration, a multi-block grid with 542976 points is generated to discrete the computational domain, the whole view and a slice view of this grid is shown in Fig.10.

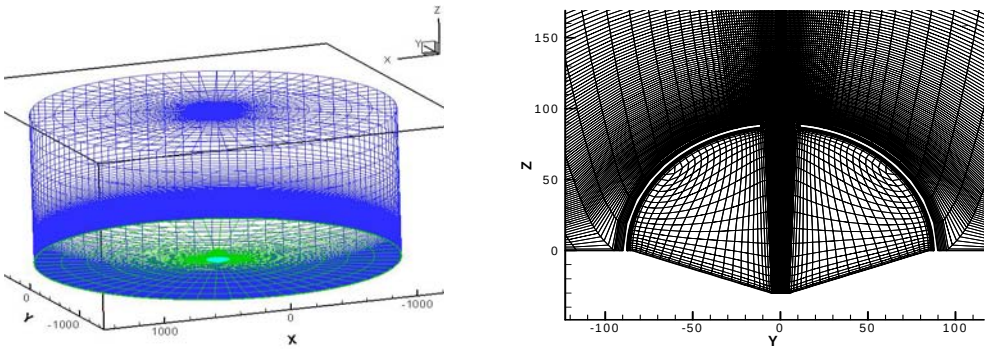


**Fig.10 Computational grid (Upper: whole grid; Lower: Slice view of x=0)**

Unsteady calculations are performed on this grid and in the calculation, a period is of ABCD vibrating is dicretized into 20 intervals, and the boundary condition of ABCD is also specified with velocity got from differentiating Eq.(6) with time. After about 10 periods'calculation, the flow field of ZNMJ reaches a periodicity. Then, the calculated streamlines in a 90mm×80mm rectangle of the x=0 slice above the jet exit at two typical moments(corresponds to the time 0 and a quarter of period in experiment) are compared with the PIV results in Fig.11 and Fig.12. It can be seen from these two figures that the calculated results agree with the experimental results qualitatively and there is a significant difference in the result of vortex distance. The reason may be attributed to the following two factors. First, the vibration amplitude of $d_{max}$=0.45mm is not directly measured but given by matching the maximum velocity in the whole flow field in computation. Second, the diaphragm of AB and CD are treated as rigid but in fact they are flexible.

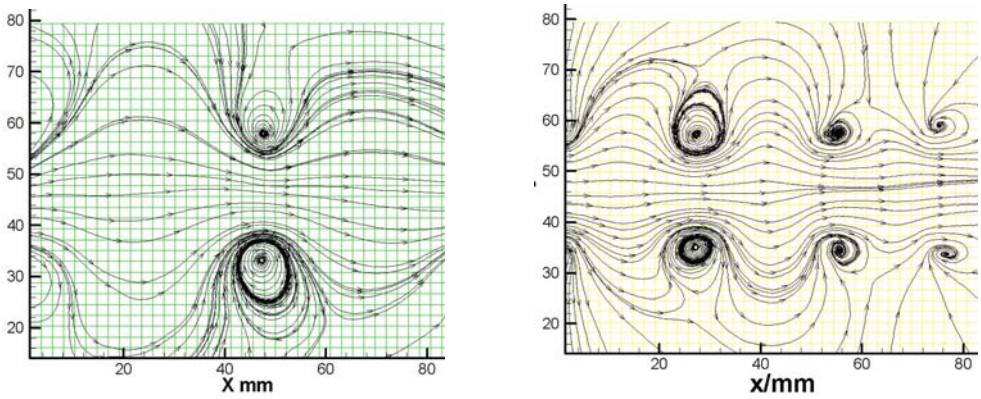


**Fig.11 Comparison of flow field ( Left:PIV, Right: Calc. )**

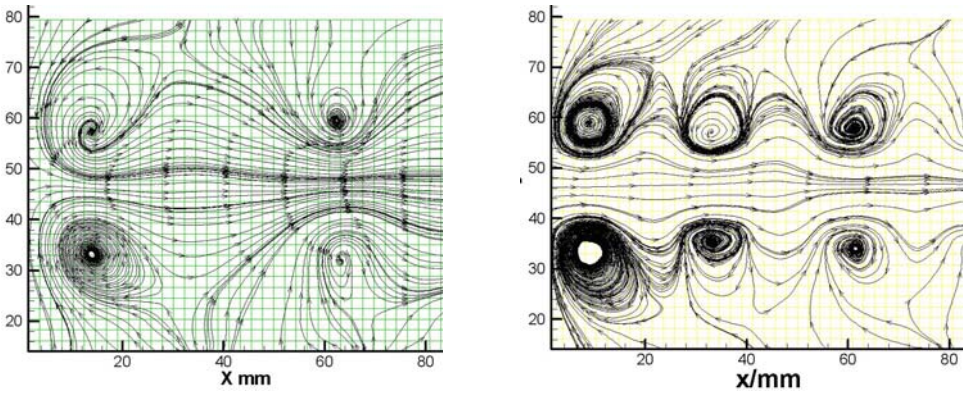


**Fig.12 Comparison of flow field ( Left:PIV, Right: Calc. )**

## CONCLUSION

In this paper, the numerical method to simulate the unsteady ZNMJ flow field is developed and applied to analyze the flow characteristics in three typical configurations of ZNMJ device. For the first configuration, the influence of Boundary Condition(BC) setting, the effect of Geometric Conservation Law(GCL) in the dynamic grid deformation technique are studied and the following two conclusions are drawn. First, when dynamic grid deformation technique is used in the unsteady flowfield simulation, only the results utilizing the GCL are rational. Second, the calculated results of dynamic grid deformation technique together with GCL is nearly identical to the results calculated by specifying a BC of time-varying velocity value to the moving boundary on the fixed grid, so that this BC specification method can be applied to complex configuration calculation for simplicity. Moreover, the flow fields of the second 2D and third 3D configuration are computed and compared to respective PIV experimental results. It is shown that the calculated results agree with the experimental results substantially and some difference exists for the "suction" phase of the ZNMJ, which needs further investigation. However, generally speaking, this developed numerical method is a feasible tool to depict the flow field of ZNMJ and can be extended for engineering practices.

## REFERENCES

Dubuc, L. et al. (1998), "Solution of the Unsteady Euler Equations Using an Implicit Dual-Time Method," AIAA Journal, 36(8), 1417-1424.

Gu, Y.S. and X. Ming (2005), "Investigation the Characteristics and Structures of Unsteady Flow Field Near The Zero-Mass Flux Jet with PIV," Journal of Experiments in Fluid Mechanics, **19**(1), 83-86 (In Chinese)

Hassan, A.A. (2001), "Application of Zero-Net-Mass Jets for Enhanced Rotorcraft Aerodynamic Performance," AIAA Journal, **38**(3), 478-485.

Luo, Z.B. (2006), Principle of Synthetic Jet and Dual Synthetic Jets and their Applications in Jet Vectoring and Micro-Pump, Ph.D thesis, National University of Defense Technology, China (In Chinese)

Menter, F.R. (1993), Zonal Two Equation Turbulence Models for Aerodynamic Flows. AIAA 93-2906, 1993

Tang, H. and S. Zhong (2006), "Incompressible Flow Model of Synthetic Jet Actuators," AIAA Journal, **44**(4), 908-912.

Zhu, Z.Q. (1998), Application of Computational Fluid Dynamics, Beijing University of Aeronautics and Astronautics Press, Beijing. (In Chinese)